Orbital stability in the spin-ordered phase of bilayer manganites as investigated by neutron-diffraction measurements

T. Akimoto
Department of Crystalline Materials Science, Nagoya University, Nagoya 464-8603, Japan

Y. Moritomo
CIRSE, Nagoya University, Nagoya 464-8601, and PRESTO, JST, Japan

K. Ohoyama, S. Okamoto, S. Ishihara, and S. Maekawa
Institute for Materials Research, Tohoku University, Sendai 980-8577, Japan

K. Hirota
Department of Physics, Tohoku University, Sendai 980-8578, Japan

A. Nakamura
CIRSE, Nagoya University, Nagoya 464-8601, Japan
(Received 1 October 1999; revised manuscript received 10 January 2000)

Temperature variation of lattice structure has been investigated for ferromagnetic $La(Sr_{0.8}Ca_{0.2})_2Mn_2O_7$ and layered-type (A-type) antiferromagnetic $NdSr_2Mn_2O_7$. We have found that distortion of the MnO_6 octahedra decreases in the spin-ordered phase for both the systems. We further estimated the relative stability of the e_g orbitals by means of Madelung potential calculation, and discussed the orbital state in the spin-ordered phase.

Doped manganites with bilayer structure,[1] $La_{2-2x}Sr_{1+2x}Mn_2O_7$, have recently attracted considerable interest due to the interrelation between magnetic structure and the orbital stability of the degenerated e_g states.[2–4] Akimoto *et al.*[5] have investigated the stability of the $d_{3z^2-r^2}$ (or $d_{x^2-y^2}$) orbital at room temperature by Madelung potential calculation[2] based on the structural data of structure-controlled $(La_{1-z}Nd_z)_{1.2}(Sr_{1-y}Ca_y)_{1.8}Mn_2O_7$ at a fixed hole concentration ($x=0.4$). They have found a strong interrelation between the orbital stability and magnetic structure: with increase of stability of the $d_{3z^2-r^2}$ orbital, the magnetic structure changes from layered-type antiferromagnetic (A-type) to ferromagnetic (F-type) ones. Recently, Takata *et al.*[6] have directly observed the $d_{x^2-y^2}$ orbital state in $NdSr_2Mn_2O_7$, analyzing x-ray-diffraction data by means of the maximum entropy method (MEM). The compound shows a layered-type (A-type) antiferromagnetic spin-ordering below $T_N \sim 150$ K, in which the ferromagnetic MnO_2 sheet alternates along the c axis (intrabilayer exchange coupling is *negative.*)[7–9] Such a magnetic structure is well understood with the $d_{x^2-y^2}$ state, which causes the ferromagnetic double-exchange interaction[10] within the MnO_2 sheet and antiferromagnetic superexchange coupling between the adjacent sheets (within the bilayer). Thus, the stability of the e_g orbital, which is governed by the lattice structure through an electrostatic manner, has significant effects on the magnetic structures of bilayer manganites.

Up to the present, many researchers have reported the lattice and magnetic structures for $La_{2-2x}Sr_{1+2x}Mn_2O_7$.[5,7–9,11–13] Especially, Argyriou *et al.*[12] and Kimura *et al.*[13] have observed lattice structural changes at the magnetic transition temperature in $La_{2-2x}Sr_{1+2x}Mn_2O_7$, suggesting variation of the orbital stability. Mitchell *et al.*[11] have investigated the temperature dependence of the distortion of the MnO_6 octahedra of $La_{1.2}Sr_{1.8}Mn_2O_7(x=0.4)$ by means of neutron-diffraction measurements. They have found that the magnitude of the Jahn-Teller distortion enhances in the ferromagnetic metallic (FM) phase. In the electrostatic point of view, the enhanced distortion of the MnO_6 octahedron stabilizes the $d_{3z^2-r^2}$ state rather than the $d_{x^2-y^2}$ state. This behavior is rather strange, since the in-plane transfer integral between the neighboring Mn sites would be suppressed with this orbital state.

Here, we have found that the 20% Ca-doped manganite, $La(Sr_{0.8}Ca_{0.2})_2Mn_2O_7$, at $x=0.5$ becomes FM below $T_C \sim 100$ K [see Fig. 2(c)]. Note that the mother material, $LaSr_2Mn_2O_7$, shows a charge-ordering (CO) transition at ~ 210 K. With decreasing temperature, the CO phase is suppressed and the low-temperature phase is dominated by the A-type spin ordering.[14] In order to investigate the orbital state in the spin-ordered phase, we have performed neutron powder-diffraction experiments on the F-type $La(Sr_{0.8}Ca_{0.2})_2Mn_2O_7$ and A-type $NdSr_2Mn_2O_7$.[8] The relative stability of the $d_{3z^2-r^2}$ and $d_{x^2-y^2}$ orbitals has been estimated by difference in the Madelung potential ΔV between the two e_g orbitals. Our results suggest that the orbital state of the FM state is a linear combination of the $d_{x^2-y^2}$ and $d_{3z^2-r^2}$ orbitals, making a sharp contrast with the $d_{x^2-y^2}$ state in the A-type spin-ordered phase.

Melt-grown crystals of $La(Sr_{0.8}Ca_{0.2})_2Mn_2O_7$ and $NdSr_2Mn_2O_7$ has been used for the neutron-diffraction measurement to reduce the impurity phase. Crystals were grown by the floating-zone method at a feeding speed of 10–20 mm/h. Stoichiometric mixture of commercial La_2O_3, Nd_2O_3, $SrCO_3$, $CaCO_3$, and Mn_3O_4 powder was ground and calcined twice at 1250–1350 for 24 h. The resulting powder was pressed into a rod with a size of 5 mm$\phi \times$80 mm and sintered at 1350 for 48 h. The ingre-

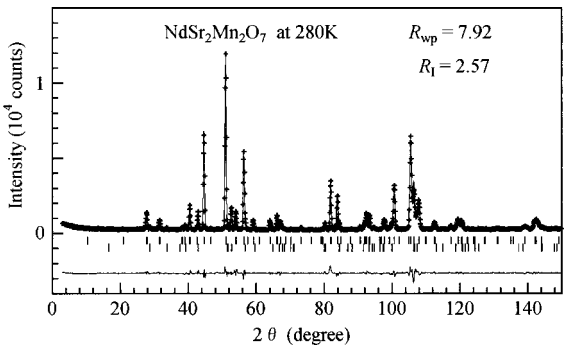

FIG. 1. The whole neutron powder diffraction patterns (cross) of $NdSr_2Mn_2O_7$ at 280 K. The solid curve is the result of the multiphase Rietveld refinement with a ''327'' main phase and a ''214'' impurity phase.

dient could be melted congruently in a flow of oxygen. Neutron-diffraction measurements were performed with the Kinken powder diffractometer for high efficiency and high-resolution measurements (HERMES) installed at the JRR-3M reactor at the Japan Atomic Energy Research Institute, Tokai, Japan.[15] Neutrons with wavelength 1.8196 Å were obtained by the 331 reflection of the Ge monochromator, and 12'$-\infty-$Sample$-$22' collimation. Diffraction angle 2θ is from 3° to 153°. Melt-grown crystal ingots were crushed into fine powder and were sealed in a vanadium capsule with helium gas, and mounted at the cold head of a closed-cycle He-gas refrigerator. The crystal symmetry is tetragonal ($I4/mmm; Z=2$) at all temperatures. We have used the RIETAN-97 program developed by Izumi,[16] and analyzed the powder patterns with the two-phase model (''327'' main phase and ''214'' impurity phase). We show in Fig. 1 prototypical results of the Rietveld refinement of $NdSr_2Mn_2O_7$ at 280 K. The final refinement is satisfactory, in which R_{wp} and R_I (reliable factor based on the integrated intensity) are fairly typical of published structures ($R_{wp}=7.92\%, R_I=2.57\%$). We listed prototypical results in Table I.

First of all, let us see the temperature variation of the F- and A-type magnetic moments. Figure 2(a) shows the A and F components for $La(Sr_{0.8}Ca_{0.2})_2Mn_2O_7$: squares and circles are for the F and A components, respectively. The magnitudes of the moments are determined by the Rietveld fitting (FAT-RIETAN), in which we assume ferromagnetic (antiferromagnetic) arrangement of the ferromagnetic MnO_2 layers. The magnetic moments lie in the MnO_2 sheets for both the components. The magnitude of the A component (open circles) increases below $T_N\sim150$ K, and becomes $\sim1\mu_B$. With further decrease of temperature, the F component appears below 100 K and increases up to $\sim3\mu_B$. Temperature variation of resistivity ρ shows a steep reduction below $T_C(\sim100$ K) [see Fig. 2(c)], indicating that the low-temperature phase of $La(Sr_{0.8}Ca_{0.2})_2Mn_2O_7$ is ferromagnetic metallic (FM) one. Coexistence of the F and A components may be ascribed to the spin canting, similarly to the case of $La_{1.2}Sr_{1.8}Mn_2O_7$.[7] Hereafter, we simply call the temperature where F component appears as T_C. Temperature variation of magnetization [M is the broken curve in Fig. 2(a)] shows a ferromagnetic behavior with saturated moment M_s of $\approx3.1\mu_B$, consistently with the Rietveld refinement. On the other hand, the A-type moment of $NdSr_2Mn_2O_7$ [see Fig. 2(b)] increases below $T_N(=110$ K), and nearly saturates ($\sim2\mu_B$) at ~50 K.[17] The broken curve represents the temperature dependence of in-plane component of susceptibility (χ_{ab}).[18]

Figure 3 shows the temperature dependence of the lattice constants, i.e., a and c, of (a) $La(Sr_{0.8}Ca_{0.2})_2Mn_2O_7$ and (b) $NdSr_2Mn_2O_7$.[19] In the case of F-type $La(Sr_{0.8}Ca_{0.2})_2Mn_2O_7$ [see Fig. 3(a)], the c value decreases below T_C. Such a behavior makes a sharp contrast with the case of $La_{1.2}Sr_{1.8}Mn_2O_7$,[11] in which the c value increases below T_C. In the A-type $NdSr_2Mn_2O_7$ [Fig. 3(b)], both the lattice constants change below T_N, indicating a significant spin-lattice

TABLE I. Lattice constants and atomic positions of $La(Sr_{0.8}Ca_{0.2})Mn_2O_7$ and $NdSr_2Mn_2O_7$ determined from the neutron powder profiles. Two-phase Rietveld analysis (''327'' main phase + ''214'' impurity phase) has been performed. The crystal symmetry is tetragonal ($I4/mmm; Z=2$). The atomic sites are $A1$ $2b$ $[0,0,\frac{1}{2}]$, A 2 $4e$ $[0,0,z]$, O12a $[0,0,0]$, O2 $4e$ $[0,0,z]$, O3 $8g$ $[0,\frac{1}{2},z]$ and Mn $4e$ $[0,0,z]$ (A is the site of the rare-earth and alkaline-earth ions). The impurity amount r is also listed.

Compound	Temperature (K)	a(Å)	c(Å)	$A2(z)$	O2(z)	O3(z)	Mn(z)
	280	3.8426(2)	19.995(1)	0.3179(3)	0.1968(4)	0.0962(2)	0.0964(5)
$NdSr_2Mn_2O_7$	120	3.8412(9)	19.931(8)	0.3183(5)	0.1962(4)	0.0961(2)	0.0959(7)
	30	3.8424(3)	19.897(5)	0.3188(6)	0.1973(4)	0.0968(3)	0.0954(7)
	300	3.8688(6)	20.213(5)	0.3172(4)	0.1968(6)	0.0963(3)	0.0949(8)
$La(Sr_{0.8}Ca_{0.2})_2Mn_2O_7$	110	3.8664(3)	20.154(6)	0.3168(5)	0.1970(7)	0.0961(4)	0.0951(8)
	50	3.8658(6)	20.126(7)	0.3168(5)	0.1966(7)	0.0960(7)	0.0950(9)

Compound	Temperature (K)	R_{wp}(%)	R_I(%)	r(%)
	280	7.92	2.57	12.5(2)
$NdSr_2Mn_2O_7$	120	9.02	2.86	13.2(3)
	30	9.81	2.55	13.3(3)
	300	10.79	2.53	27.5(7)
$La(Sr_{0.8}Ca_{0.2})_2Mn_2O_7$	110	12.62	2.46	29(1)
	50	12.89	2.67	28.4(9)

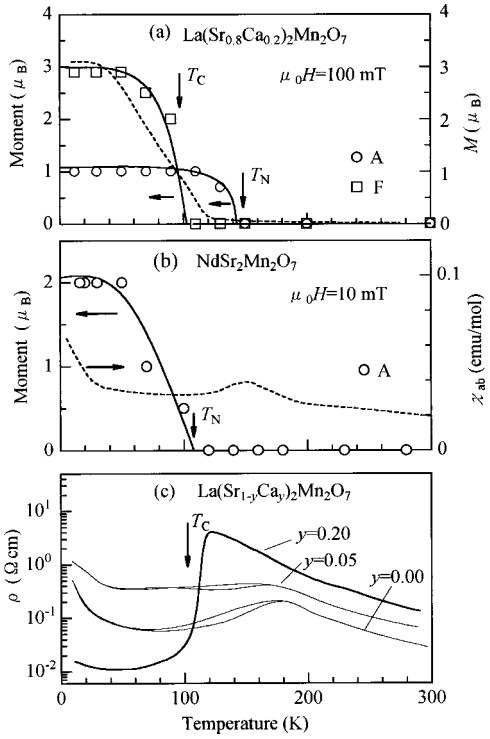

FIG. 2. Temperature dependence of magnitude of the ferromagnetic (F) and antiferromagnetic (A) components of (a) $La(Sr_{0.8}Ca_{0.2})_2Mn_2O_7$ and (b) $NdSr_2Mn_2O_7$. T_C and T_N represent the critical temperatures for the ferromagnetic and antiferromagnetic transition, respectively. The broken curve in (a) is the magnetization (M), which was measured in the field of 100 mT after cooling down to 5 K in the zero field (ZFC). The broken curve in (b) is the in-plane component of susceptibility (χ_{ab}) at 10 mT measured under the ZFC condition. (c) The temperature variation of resistivity ρ of melt-grown $La(Sr_{1-y}Ca_y)Mn_2O_7$ crystal. Thin curves ($y=0.00$ and $y=0.05$) are the in-plane component of ρ.

coupling. Here, we investigate the details of the lattice structural change induced by magnetic ordering. We show in Fig. 4 three kinds of Mn-O bondlengths, i.e., out-of-plane [$d_{\text{Mn-O(1)}}$ and $d_{\text{Mn-O(2)}}$; O(1) locates at the central position in the bilayer, while O(2) locates at the outer side of the bilayer] and in-plane ($d_{\text{Mn-O(3)}}$) bondlengths, of (a) $La(Sr_{0.8}Ca_{0.2})_2Mn_2O_7$ and (b) $NdSr_2Mn_2O_7$. In $La(Sr_{0.8}Ca_{0.2})_2Mn_2O_7$ [Fig. 4(a)], $d_{\text{Mn-O(2)}}$ (closed circles)

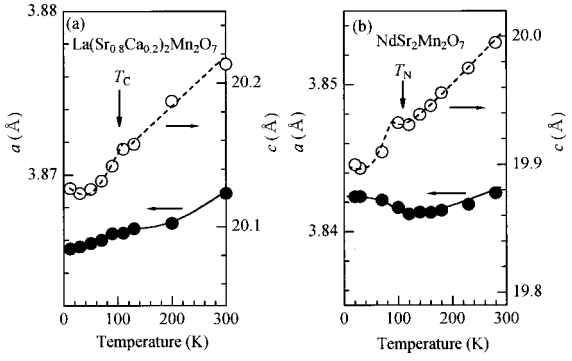

FIG. 3. Temperature variation of lattice constants of (a) $La(Sr_{0.8}Ca_{0.2})_2Mn_2O_7$ and (b) $NdSr_2Mn_2O_7$. $T_C(T_N)$ represents the critical temperature for the ferromagnetic (antiferromagnetic) transition.

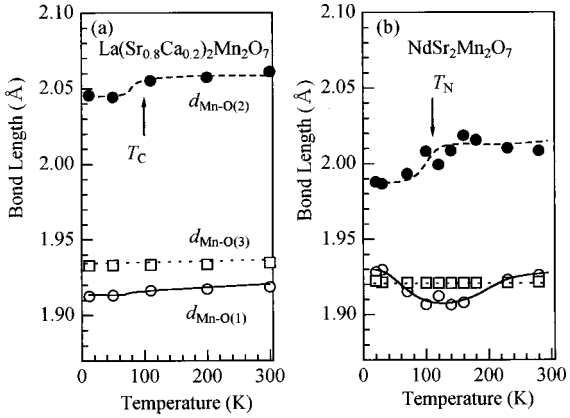

FIG. 4. Temperature variation of the Mn-O bondlengths of (a) $La(Sr_{0.8}Ca_{0.2})_2Mn_2O_7$ and (b) $NdSr_2Mn_2O_7$. T_C (T_N) represents the critical temperature for the ferromagnetic (antiferromagnetic) transition. $d_{\text{Mn-O(1)}}$ and $d_{\text{Mn-O(2)}}$ are the out-of-plane bondlengths, and $d_{\text{Mn-O(3)}}$ is the in-plane bondlength.

becomes shorter below T_C. Such a shrinkage of the $d_{\text{Mn-O(2)}}$, or the release of the Jahn-Teller-type distortion of the MnO_6 octahedra, is opposite to the case of $La_{1.2}Sr_{1.8}Mn_2O_7$.[11] On the other hand, in $NdSr_2Mn_2O_7$ [Fig. 4(b)], $d_{\text{Mn-O(1)}}$ (open circles) elongates and $d_{\text{Mn-O(2)}}$ (closed circles) shrinks below T_N.

Now, let us proceed to the relative stability of the e_g orbitals. The orbital stability can be evaluated by the Madelung potentials[2,20] for the $d_{x^2-y^2}$ and $d_{3z^2-r^2}$ orbitals.[5] The Madelung potentials acting on a hole in the $d_{x^2-y^2}$ and $d_{3z^2-r^2}$ orbitals are given by $V(d_{x^2-y^2})=V(\vec{r_0}+r_d\hat{x})$, and $V(d_{3z^2-r^2})=[V(\vec{r_0}+r_d\hat{z})+V(\vec{r_0}-r_d\hat{z})]/2$, respectively. Here $\vec{r_0}$ indicates the position of the Mn ion and $r_d(=0.42$ Å) is the radius where the radial charge density of the $3d$ orbital becomes maximum. $\hat{x}$ and $\hat{z}$ are the unit vectors along the crystallographic a and c axes, respectively. Based on the structural data obtained by the neutron-diffraction experiment, we have calculated the temperature variation of the difference of the Madelung potentials between two e_g orbitals: $\Delta V=V(d_{3z^2-r^2})-V(d_{x^2-y^2})$. The $d_{x^2-y^2}$ orbital becomes stable as ΔV decreases. The results are plotted in Fig. 5 together with the data points (closed squares) for the F-type $La_{1.2}Sr_{1.8}Mn_2O_7$.[9] With decrease of temperature, the ΔV value (closed circles) of $La(Sr_{0.8}Ca_{0.2})_2Mn_2O_7$ gradually decreases, and hence the $d_{x^2-y^2}$ orbital becomes stable. Oppositely to this case, the ΔV value (closed squares) of $LaSr_2Mn_2O_7$ rather increases (the $d_{3z^2-r^2}$ orbital becomes stable) at low temperature. Here, we should mention that ΔV values for both the ferromagnetic systems converge at $\sim$0.06–0.07 eV at the lowest temperature. This suggests that the orbital state in the FM phase is a linear combination of the $d_{x^2-y^2}$ and $d_{3z^2-r^2}$ orbitals. On the other hand, the ΔV value of the A-type $NdSr_2Mn_2O_7$ steeply decreases below $T_N(=110$ K) down to 0.02 eV. Such a large reduction of the ΔV value suggests that the $d_{x^2-y^2}$ orbital dominates in the A-type antiferromagnetic phase, consistently with the MEM analysis on $NdSr_2Mn_2O_7$.[6]

The orbital mixing in the FM state can be ascribed to the subtle balance between the three-dimensional (3D) double-exchange interaction mediated by the e_g electrons and the

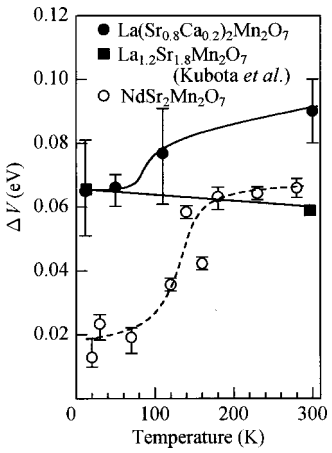

FIG. 5. Temperature variation of difference of the Madelung potentials $\Delta V[\equiv V(d_{3z^2-r^2})-V(d_{x^2-y^2})]$, where $V(d_{3z^2-r^2})[V(d_{x^2-y^2})]$ is the Madelung potential for the $d_{3z^2-r^2}(d_{x^2-y^2})$ hole. The $d_{x^2-y^2}$ orbital becomes stable as ΔV decreases. Closed circles, closed squares, and open circles stand for $La(Sr_{0.8}Ca_{0.2})_2Mn_2O_7$, $La_{1.2}Sr_{1.8}Mn_2O_7$, and $NdSr_2Mn_2O_7$, respectively. Structural parameters of $La_{1.2}Sr_{1.8}Mn_2O_7$ were obtained from Ref. 9.

kinetic energy gain of the e_g-electron system. To realize the 3D double-exchange coupling,[10] the e_g electrons should hop both to the in-plane and out-of-plane directions. Then, the e_g electrons should share the $d_{3z^2-r^2}$ character, since the $d_{x^2-y^2}$-electron has zero transfer integral between the adjacent MnO_2 sheets. The kinetic energy of the e_g-electron system, however, fairly loses with the perfect $d_{3z^2-r^2}$ polarization.[21] Accordingly, optimal mixing of the $d_{x^2-y^2}$ and $d_{3z^2-r^2}$ orbitals is realized to minimize the total energy of the 3D FM phase. Such a picture on the orbital state is consistent with the chemical pressure effect on the bilayer manganites:[5] with an increase of stability of the $d_{3z^2-r^2}$ orbital, the low-temperature phase changes from the A-type antiferromagnetic, and the FM to paramagnetic insulating ones. Okamoto *et al.*[3] have theoretically investigated the orbital state of bilayer manganites based on the double-exchange Hamiltonian with explicitly taking into account the orbital anisotropy. Consistently with our experimental results, they have obtained an orbital state of the linear combination of the $d_{x^2-y^2}$ and $d_{3z^2-r^2}$ orbitals.

In summary, we have investigated the orbital states of bilayer manganites by means of Madelung potential calculation based on the structural parameters. The obtained results suggest that the FM phase is the mixed state of the $d_{x^2-y^2}$ and $d_{3z^2-r^2}$ orbitals, making a sharp contrast with the $d_{x^2-y^2}$ state in the A-type antiferromagnetic phase of $NdSr_2Mn_2O_7$. Thus, the orbital state is strongly coupled with the spin state in the bilayer manganites. To understand the physics of the doped manganites in a true sense, detailed investigations on the orbital states is indispensable.

The authors are grateful to K. Nemoto for his help in the measurement of neutron powder diffraction. S.O. and T.A. acknowledge the financial support of JSPS. This work was supported by a Grant-In-Aid for Scientific Research from the Ministry of Education, Science, Sports, and Culture, from Precursory Research for Embryonic Science and Technology (PRESTO), Japan Science and Technology Corporation (JST).

[1] Y. Moritomo, A. Asamitu, H. Kuwahara, and Y. Tokura, Nature (London) **380**, 141 (1996).
[2] S. Ishihara, S. Okamoto, and S. Maekawa, J. Phys. Soc. Jpn. **66**, 2965 (1997).
[3] S. Okamoto *et al.* M.S. thesis, Nagoya University, 1998.
[4] R. Maezono and N. Nagaosa, Phys. Rev. B **61**, 1825 (2000).
[5] T. Akimoto, Y. Moritomo, K. Ohoyama, S. Okamoto, S. Ishihara, S. Maekawa, and A. Nakamura, Phys. Rev. B **59**, R14 153 (1999).
[6] M. Takata, E. Nishibori, K. Kato, M. Sakata, and Y. Moritomo, J. Phys. Soc. Jpn. **68**, 2190 (1999).
[7] K. Hirota, Y. Moritomo, H. Fujioka, M. Kubota, H. Yosizawa, and Y. Endo, J. Phys. Soc. Jpn. **67**, 3380 (1998).
[8] Y. Moritomo, A. Nakamura, K. Ohoyama, M. Ohasi, and K. Hirota, J. Phys. Soc. Jpn. **68**, 631 (1999).
[9] M. Kubota, H. Yoshizawa, K. Hirota, H. Fujioka, Y. Endo, and Y. Moritomo, J. Phys. Chem. Solids **60**, 1161 (1999); M. Kubota, H. Fujioka, K. Hirota, K. Ohoyama, Y. Moritomo, H. Yoshizawa, and Y. Endo, cond-mat/9902288 (unpublished).
[10] P.W. Anderson and H. Hasagawa, Phys. Rev. **100**, 675 (1955).
[11] J.F. Mitchell, D.N. Argyriou, J.D. Jorgensen, D.G. Hinks, C.D. Potter, and S.D. Bader, Phys. Rev. B **55**, 63 (1997).
[12] D.N. Argyriou, J.F. Mitchell, C.D. Potter, S.D. Bader, R. Kleb, and J.D. Jorgensen, Phys. Rev. B **55**, R11 965 (1997); D.N. Argyriou, J.F. Mitcell, J.B. Goodenough, O. Chmaissem, S. Short, and J.D. Jorgensen, Phys. Rev. Lett. **78**, 1568 (1997); D.N. Argyriou, J.F. Mitchell, P.G. Radaelli, H.N. Bordallo, D.E. Cox, M. Medarde, and J.D. Jorgensen, Phys. Rev. B **59**, 8695 (1999).
[13] T. Kimura, Y. Tomioka, A. Asamitsu, and Y. Tokura, Phys. Rev. Lett. **81**, 5920 (1998).
[14] M. Kubota, H. Yoshizawa, Y. Moritomo, H. Fujioka, K. Hirota, and Y. Endo, J. Phys. Soc. Jpn. **68**, 2202 (1999).
[15] K. Ohoyama, T. Kanouchi, K. Nemoto, M. Ohashi, T. Kajitani, and Y. Yamaguchi, Jpn. J. Appl. Phys., Part 1 **37**, 3319 (1998).
[16] F. Izumi, *The Rietveld Method*, edited by R. A. Young (Oxford University Press, Oxford, 1993), Chap. 13; Y.-I. Kim and F. Izumi, J. Ceram. Soc. Jpn. **102**, 401 (1994).
[17] Below 50 K, the spin moments rotate toward the *c* axis (Ref. 8).
[18] One may find a broad maximum at ~150 K in the $\chi_{ab}-T$ curve shown in Fig. 2(a), which has been ascribed to the antiferromagnetic transition (Ref. 8). The present neutron experiment, however, has revealed that T_N is rather lower (~110 K).
[19] The lattice constants are slightly different from the data reported by Battle *et al.* [Phys. Rev. B **54**, 15 967 (1996)]. This is probably due to the different sample preparation procedure as well as the different multi-phase Rietveld analysis.
[20] Y. Ohta, T. Tohyama, and S. Maekawa, Phys. Rev. B **43**, 2968 (1991).
[21] The e_g-electron system gains the maximum kinetic energy with the $d_{x^2-y^2}$ polarization.